

Bioinduced precipitation of barite and celestite in dolomite microbialites

Examples from Miocene lacustrine sequences in the Madrid and Duero Basins, Spain

M. Esther Sanz-Montero ^{a,b,*}, J. Pablo Rodríguez-Aranda ^a, M. Angeles García del Cura ^{b,c}

^a Dpto. Petrología y Geoquímica, Facultad de Ciencias Geológicas, UCM, 28040 Madrid, Spain

^b Instituto de Geología Económica (CSIC-UCM), C/Antonio Novais, 2, 28040 Madrid, Spain

^c Laboratorio de Petrología Aplicada, Unidad asociada CSIC-UA. 03080 Alicante, Spain

This paper provides an ancient analogue for biologically mediated celestite and barite formation in dolomite precipitating microbial mats developed in lacustrine environments during the Miocene. Barite and celestite occurrences were studied in three temporally and spatially separated sedimentary successions: S1 and S2 in the Madrid Basin and S3 in the Duero Basin. In S1, macrocrystalline selenite gypsum occurs as laterally continuous beds; in the two other successions (S2 and S3), calcite pseudomorphs of lenticular gypsum aggregates are hosted in dolomite beds as evidence for the former presence of this evaporite. In S1, only celestite is associated with dolomite. Celestite crystals occur as both intergrown clusters, concentrated in pockets likely created by the dissolution of intrasedimentary anhydrite precursors, and as single precipitates associated with dolomite masses that replace selenite gypsum. Celestite crystals are nucleated commonly on organic substances that are pervasively associated with them. In S2 and S3, scarce single celestite crystals are restricted to calcite pseudomorphs after gypsum, whereas barite is the sulphate precipitated in the pseudomorphs' surroundings. Barite is commonly present as patchy poikilitic crystals which include microbial structures and is embedded in organic matter. Additionally, barite is found as a secondary precipitate within Ba-bearing feldspars. Feldspar weathering is, thus, envisaged as a major source of barium at these sites. Petrographical, isotopic and compositional observations point out that the barite and celestite formation was not caused by abiological processes only. Rather, the patchy distribution of the sulphates, close links to organic matter with biogenic isotope signatures, and inclusion of microbial structures, such as biologically mediated dolomite, provides evidence for the involvement of microbes in the formation of the sulphates. The coprecipitation of barite and celestite with dolomite entails complex interactions between different microorganisms and reinforces the biological formation of dolomite in saline lakes.

Keywords: Microbialites, Biomarkers, Sulphates, Lake deposits, Tertiary

1. Introduction

Celestite (SrSO_4) is a mineral rarely found in sedimentary deposits other than evaporites, replaced evaporites, or insoluble residues of evaporites, whereas the related mineral barite (BaSO_4) is not restricted (West, 1973). Two main hypotheses have been proposed for the origin of large, sediment-hosted celestite deposits (Hanor, 2004): (1) syngenetic precipitation of celestite from evaporating water; and (2) epigenetic replacement of carbonates and calcium sulphates involving Sr-rich formation waters. However, recent findings tie minor celestite occurrences with microbial microenvironments. Experiments carried out by Schultze-Lam and Beveridge (1994) led to the epicellular precipitation of celestite on unicellular cyanobacteria. Douglas (2002)

also found that celestite formed in the exopolymers surrounding purple sulphur bacteria in microbial mats from a Bahamian hypersaline pond. A study of gypsum-hosted endoliths in Death Valley, California (Douglas and Yang, 2002) revealed that organisms were able to precipitate Sr-rich minerals, such as celestite and carbonates, within the layered community. Each mineral type was segregated into a restricted chemical zone together with a specific microbe that helped to create the chemical conditions present at that particular depth in the community (Douglas, 2005). In addition, Taberner et al. (2002) interpreted celestite as a by-product of sulphate reducing bacteria in Eocene reefs and basinal sediments of NE Spain.

Similarly, sedimentary barite has been extensively studied for palaeoenvironmental reconstruction because of its links with marine productivity (i.e., Hanor, 2000). Less well known are the barite deposits found in terrestrial surface environments, mainly in microbially colonized habitats, such as spring and lake environments (Arenas et al., 2000; Senko et al., 2004; Bonny and Jones, 2007). Traditionally,

* Corresponding author. Dpto. Petrología y Geoquímica, Facultad de Ciencias Geológicas, UCM, 28040 Madrid, Spain. Fax: +34 915442535.
E-mail address: mesanz@geo.ucm.es (M.E. Sanz-Montero).

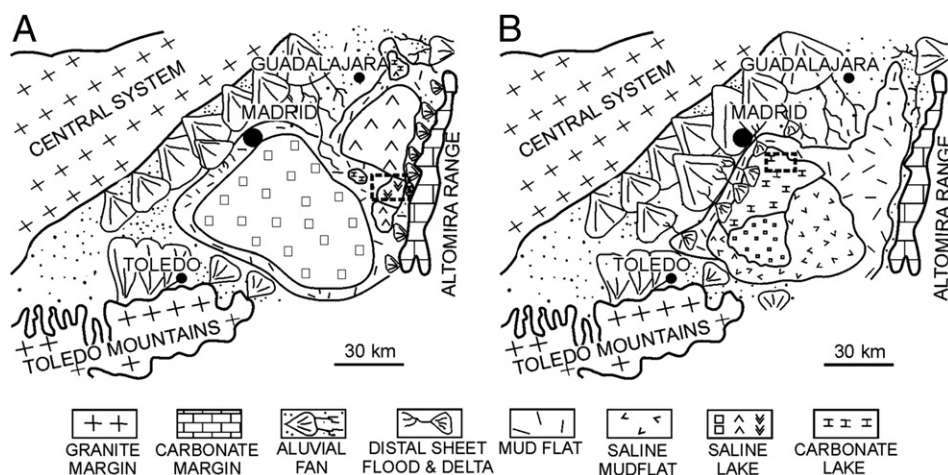


Fig. 1. Palaeogeographic sketches of the Madrid Basin with location of the study areas (squared) for the Lower (A) and Intermediate (B) Miocene Units, S1 and S2, respectively. Modified from Rodríguez-Aranda (1995) and Calvo et al. (1996).

two general abiotic mechanisms have been proposed for their formation. In the first case, barium and sulphide-laden brines mix with oxidizing meteoric water, resulting in abiotic oxidation of sulphide to sulphate which results in diagenetic barite formation (Plummer, 1971). In the second mechanism, barium-laden brines may mix with sulphate-containing meteoric water, also resulting in barite formation (Kaiser et al., 1987; Williams-Jones et al., 1992). Alternatively, recent papers have shown that sulphur-metabolizing microbes are capable of mediating barite saturation (e.g., González-Múñoz et al., 2003; Senko et al., 2004) and controlling the textural development of barite (Bonny and Jones, 2008).

This paper describes the occurrences of barite and celestine in Miocene lacustrine dolomite microbialites associated with gypsum deposits, and suggests that microbes played a role in their precipitation. Thus, this research extends previous experimental studies and work done in recent deposits to ancient rock. The presence of barite and/or

celestine in three temporally and spatially-separated, dolomitic micro-bialite-bearing successions provides an excellent opportunity to investigate the formation of these minerals under a range of situations representative of saline lake environments. Additionally, the overlap of features, distribution patterns, and relationships between the minerals over the three sedimentary successions improves the reliability of the results.

2. Geological setting and descriptions of the studied outcrops

Barite and celestine occurrences were studied in three temporally and spatially-separated, dolomitic microbialite-bearing successions. Two of these successions are located in the Madrid Basin (S1 and S2) and the third (S3) in the central part of the Duero Basin (Figs. 1 and 2) of Spain.

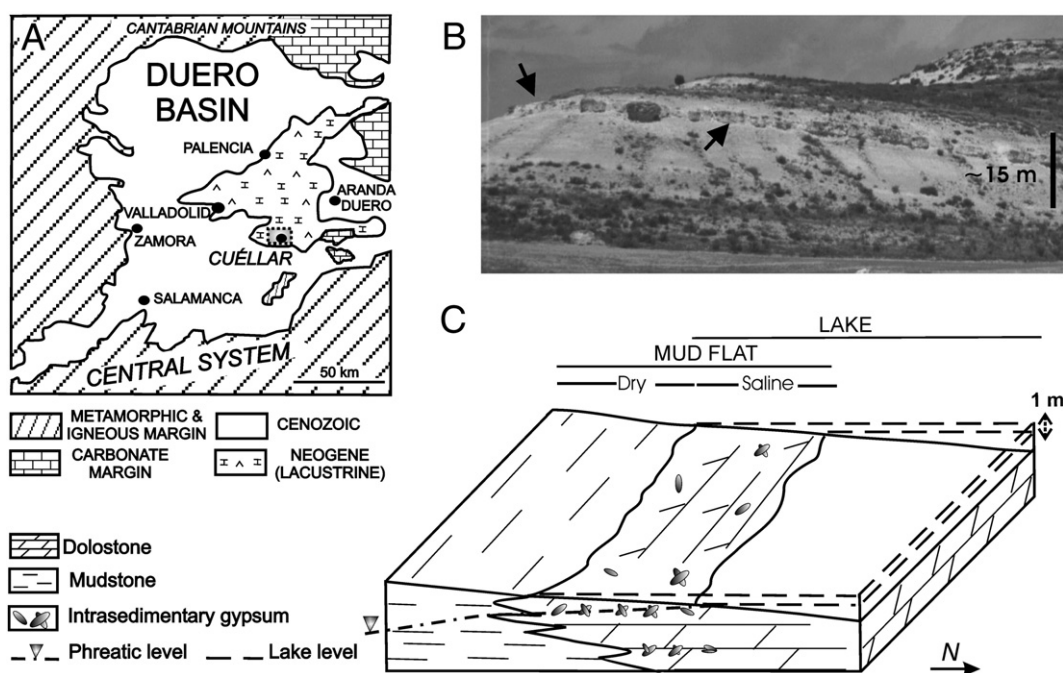


Fig. 2. A) Geological sketch of the Duero Basin with location of the study area (squared). B) Outcrop view of the pseudomorph-bearing dolomite interval (S3), which is located in the middle part of the stratigraphical section. The prominent bed (arrowed) consists of densely-packed calcite pseudomorphs after gypsum. C) Sedimentary sketch of the studied facies association, modified from Sanz-Montero et al. (2008).

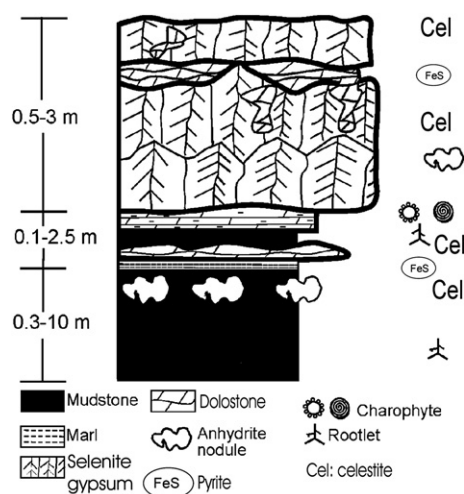


Fig. 3. Typical facies association of succession S1 (Lower Unit, Madrid Basin).

2.1. Madrid Basin

The up to 2000 m thick Miocene stratigraphical record of the Madrid Basin is divided into three main lithostratigraphic units, each separated by unconformities from their underlying units (Calvo et al., 1996). In many cases these unconformities are defined by paleokarstic surfaces (Rodríguez-Aranda et al., 2002). The two sedimentary successions studied are included in the Lower (Ramblian and early Aragonian) and Intermediate Units (Aragonian to Early Vallesian), respectively. The general sedimentary context for these units is established as mudflat-saline lake systems characteristic of a hydro-logically closed basin. The Lower Unit is composed of saline minerals (mostly glauberite, gypsum, anhydrite and halite) that were accumulated in a perennial hypersaline lake located in the basin centre and also in more diluted peripheral lakes developed close to the eastern margin (Rodríguez-Aranda et al., 1995) (Fig. 1). These evaporitic facies interfinger with carbonate, marl, and terrigenous deposits. In most of the Intermediate Unit, the lacustrine facies consist predominantly of carbonate and gypsum, which occur interbedded with mudstones in marginal areas of the lake system. Lakes developed during the sedimentation of this Unit are interpreted as shallow, slightly saline, ephemeral or perennial lakes (Calvo et al., 1996).

The studied successions S1 and S2 are located in the eastern (Lower Unit) and central areas of the Madrid Basin (Intermediate Unit), respectively (Fig. 1). The first succession (S1) is 50 m thick and consists mainly of selenite gypsum, dolostones, mudstones, and gypsum nodules after anhydrite hosted in dolostones and mudstones (Fig. 3) (Sanz-Montero et al., 2006a). Dolostones are present as both carbonate beds

intercalated with selenite gypsum and mudstones, locally showing domal and pustular stromatolite structures, and patches replacing macrocrystalline gypsum. The second succession (S2), included in the basal part of the Intermediate Unit, is 20 m thick and is mostly composed of dolostones, dolostones with intrasedimentary calcite pseudomorphs after gypsum, mudstones, and chert beds (Fig. 4).

2.2. Duero Basin

The Tertiary Duero Basin is located in the northwestern region of the Iberian Peninsula (Fig. 2A). According to Armenteros et al. (2002), seven main sedimentary stages or lithostratigraphic units have been distinguished in the up to 3000 m thick sedimentary record of the basin. The study succession, located near the village of Cuéllar, was deposited during the Middle-Late Miocene (equivalent to the sedimentary stage "5", defined by Armenteros et al., 2002). The up to 80 m thick stratigraphical section has been described in detail by Sanz-Montero et al. (2008). The present study is focused on a 15 m thick interval (S3) that overlies the 35 m thick basal part of the section (Fig. 2B). This laterally persistent interval consists of dolostones interbedded with dolostone-bearing intrasedimentary calcite pseudomorphs after rosette-like gypsum, and locally contains chert and mudstone facies (Fig. 4) that were formed in a mudflat-saline lake complex (Sanz-Montero et al., 2008). Displacive gypsum precipitated in soft dolomite along lake margins that were subjected to seasonal fluctuations of the water table (Fig. 2C). The lake deposits interfinger with terrigenous facies towards the basin margins in accordance with a typical alluvial-saline lake concentric pattern (Armenteros et al., 2002).

3. Methods

The mineralogy of the samples from the three successions was determined by X-ray diffraction (XRD) of powdered samples on a Philips X-ray diffraction system. Optical and fluorescence examinations were performed using an Olympus BX51 microscope with a white light source and a green-ultraviolet filter, respectively. For high-resolution textural analysis, carbon-coated thin sections and fresh broken surfaces of previously air-dried samples were studied with scanning electron microscopy provided with X-ray energy-dispersive spectroscopy, SEM-EDS (JEOL JSM-840). To obtain more precise elemental analysis, uncoated polished surfaces were examined with HITACHI S-3000N equipment operated in low vacuum. Both secondary electron (SE) and backscattered electron (BSE) images were collected. Cut, polished and carbon-coated thin sections were prepared for elemental mapping and analysis (as wt.%) on a JEOL Superprobe JXA 8900-M (EMP) equipped with four crystals spectrometers. Beam diameter was between 2 and 5 μm to minimize damage from the electron beam.

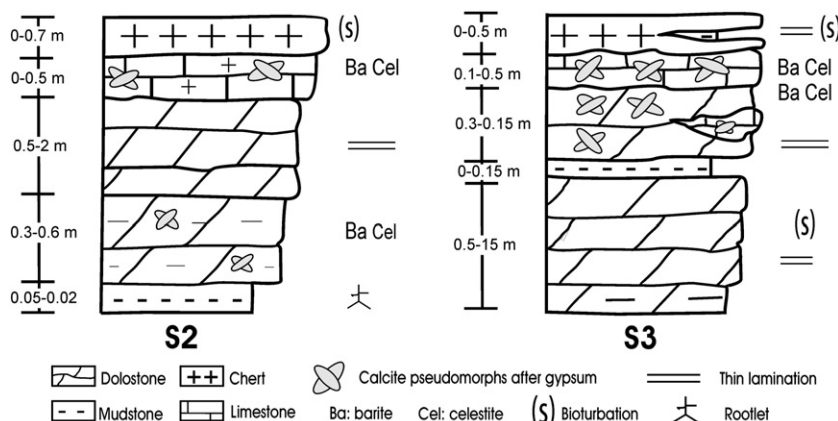


Fig. 4. Typical facies associations of the successions S2 (left, Intermediate Unit, Madrid Basin) and S3 (right, Duero Basin).

Total organic carbon (TOC) determinations in 20 bulk samples and the carbon isotope composition of 18 samples enriched in C were carried out by the Stable Isotope Laboratories of the Royal Holloway University of London, following the general analytical technique described by Grassineau (2006). The instrumentation used was a VG/Fisons/Micromass Isochrom-Elemental Analyzer system. Isotope ratios for carbon are expressed using the δ notation relative to PDB.

4. Results

4.1. Dolomite occurrences

Celestite and/or barite-bearing dolostones are commonly present in the three study successions as laterally continuous, tabular, centimetre- to decimetre-thick beds. The beds, white to cream in colour, are generally porous and friable and can be superimposed in metric sequences (Fig. 2B). The internal structure of the dolostone beds ranges from massive to vaguely laminated (Fig. 5A) and locally is disrupted by intrasedimentary gypsum. In S1, dolomite is also present as patches replacing macrocrystalline gypsum (Fig. 5B). In S2 and S3 some dolostone beds include moulds of displacive lenticular gypsum crystals, either empty or filled by cements of calcite (Fig. 6). Additionally, gypsum moulds commonly occur coated by a rim of calcite crystals. The meso-to-macrocrystalline calcite pseudomorphs after gypsum form rosette-like aggregates that occur interspersed in the

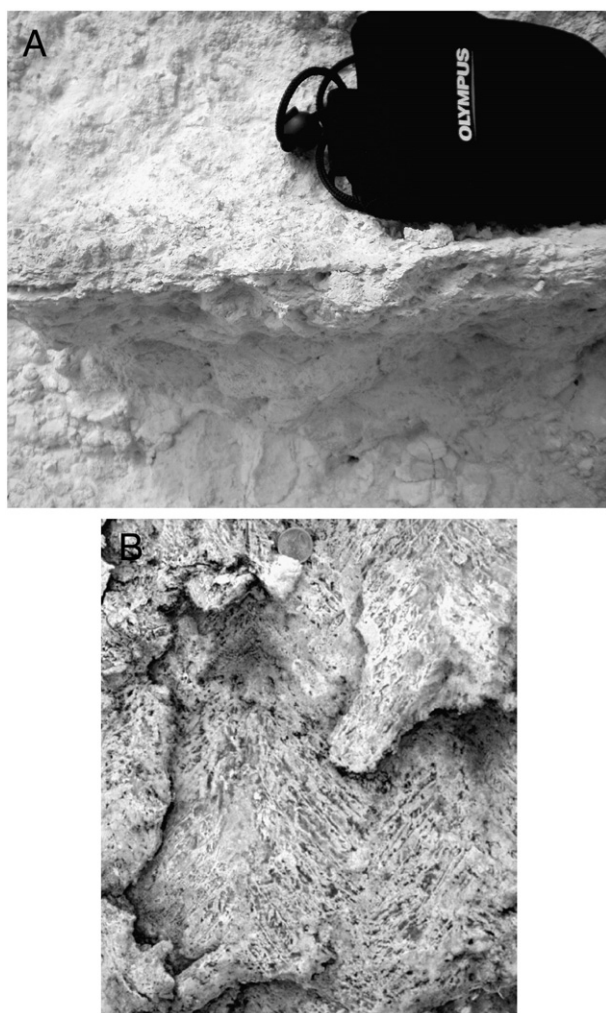


Fig. 5. Outcrop photographs. A) Massive to crudely laminated dolostone beds (S3). Case for scale 120 mm. B) Gypsum selenite crystals partially replaced by dolomite (S1). Coin for scale 22 mm.

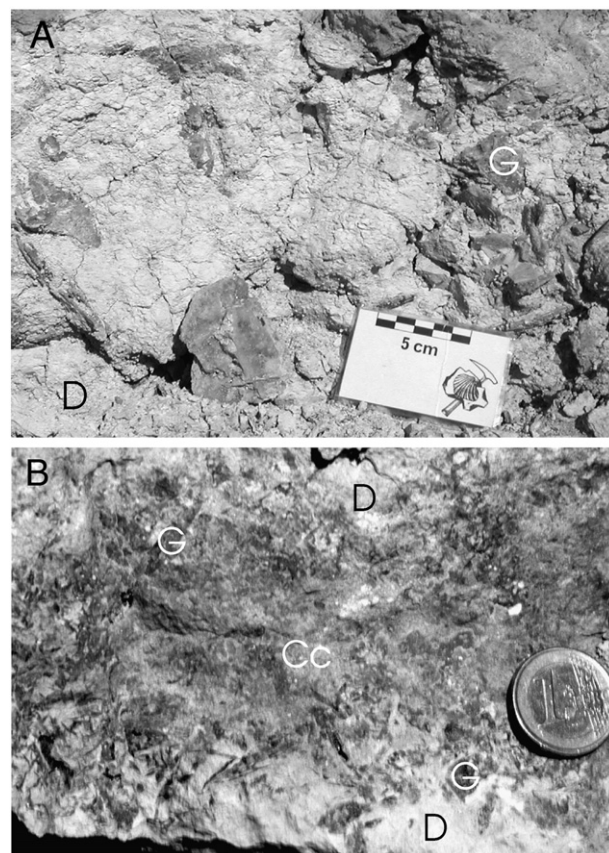


Fig. 6. Outcrop photographs of dolomite-hosted gypsum pseudomorphs (G). A) Friable dolomite (D) embedding interspersed calcite pseudomorphs after gypsum (S2). B) Dolomite (D) with intrasedimentary gypsum pseudomorphs surrounded by calcite cements (Cc), S3.

dolomite (Fig. 6A) or as prominent contorted beds 10–50 cm thick. Some of the latter crop out as protuberant and porous limestone beds (Fig. 2B) due to the abundance of calcite crystals precipitated in the pseudomorphs' surroundings (Fig. 6B). Fine-sized detrital grains (10–200 μm) are commonly found scattered throughout the dolomite. X-ray and petrographical analyses identify these as quartz, feldspar (K-feldspar and plagioclase), and phyllosilicate (muscovite, biotite, chlorite and illite). Some beds are composed of variable mixtures of dolomite and silica (opal CT and quartz).

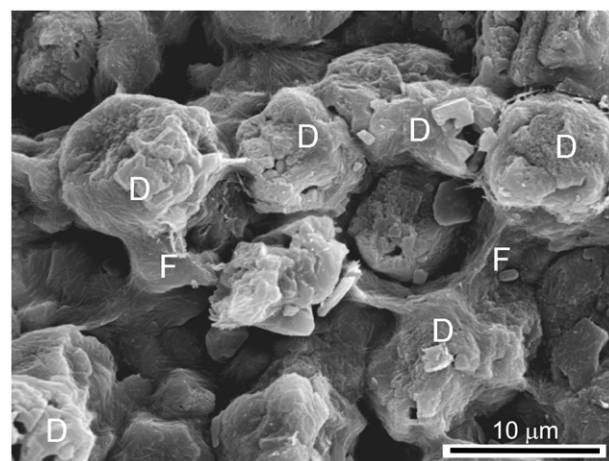


Fig. 7. SEM photograph of a freshly broken sample showing dolomite crystals (D) bonded together in a honeycomb arrangement. Each crystal is composed of stacked subcrystals and surrounded by carbonaceous films (F).

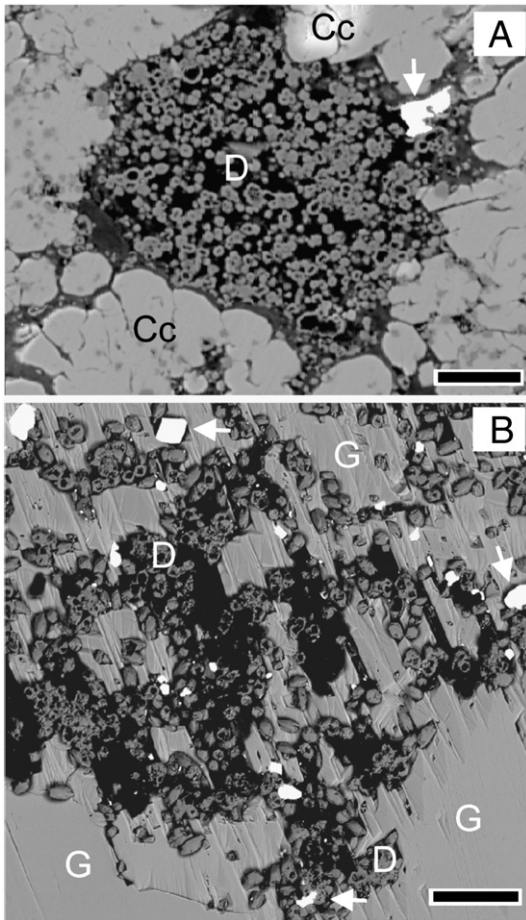


Fig. 8. SEM-BSE thin-section photomicrographs showing openly-packed dolomite crystals (D) with hollow spheroid cores. A) Barite (arrowed) embedded in dolomite is cemented by spherulite-like calcite crystals (Cc). B) Celestite crystals (white minerals, some arrowed) are associated with the dolomite replacing gypsum crystals in S1 (G). Scale bar 20 μm .

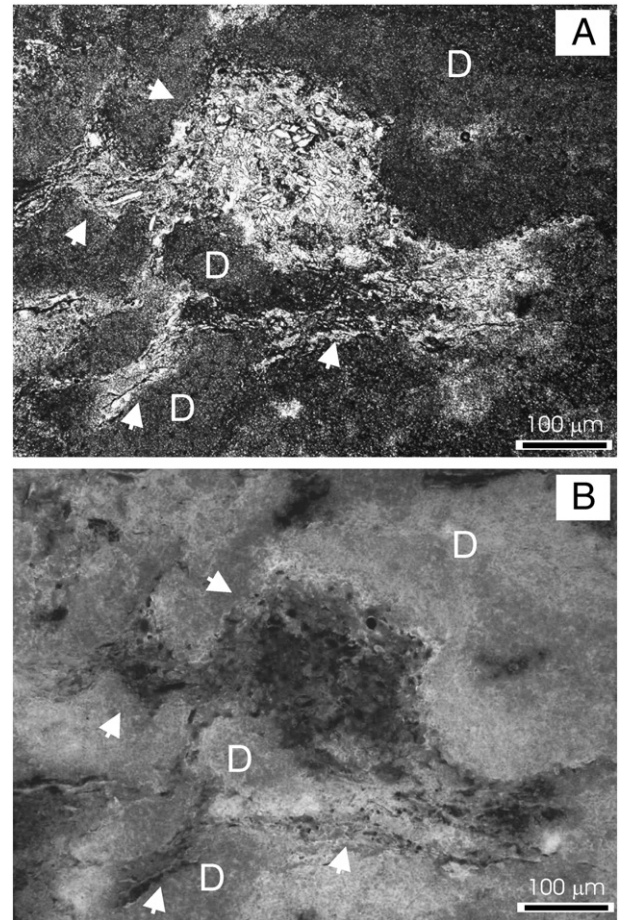


Fig. 9. Thin-section photomicrographs showing clusters of celestite crystals, concentrated in nodules and cracks (arrowed), within a dolomite matrix (D). A) Plane light. B) Same area, viewed using an UV-green filter. Non-fluorescent celestite crystals are embedded in a fluorescent dolomite groundmass.

According to previous work by Sanz-Montero et al. (2006a), Sanz-Montero et al. (2006b), Sanz-Montero et al. (2008), and Sanz-Montero et al. (2009), dolomite microfacies mainly consists of boundstones, characterised by shrub, clotted, and filament-like micrite and micro-sparite, and includes significant amounts of organic matter composed

of optically amorphous material. Due to the presence of organic matter in the carbonate, the crystals are luminescent when observed with fluorescence microscopy. Under SEM, the texture of the dolomite is characterised by open clusters of porous, micrometre-sized crystals that are commonly interwoven with bundles of organic substances (Figs. 7 and 8). Dolomite crystals are made of clusters of subcrystals

Table
Mineralogical and compositional data of the dolomite, organic carbon, and main associated minerals in the different study successions.

		Madrid Basin successions		Duero Basin succession
		S1	S2	S3
Dolomite ($n = 35$)	%CaCO ₃	49–55.2	50–52	50.3–53.7
	Crystalline order	0.29–0.62 av = 0.46	0.2–0.64 av = 0.47	0.25–0.67 av = 0.43
	$\delta^{13}\text{C}_{\text{PDB}}$ (‰)	(–7.35)–(–4.67) av = –6.60	(–5.1)–(–4.2) av = –4.6	(–6.38)–(–3.58) av = –4.83
	$\delta^{18}\text{O}_{\text{PDB}}$ (‰)	(–7.99)–(–2.65) av = –3.35	(–3.1)–(–0.3) av = –1.7	(–1.33)–(1.88) av = –0.3
	TOC (wt.%)	0.01–0.28 av = 0.10	0.03–0.10 av = 0.05	0.03–0.3 av = 0.10
Organic carbon ($n = 18$)	$\delta^{13}\text{C}_{\text{PDB}}$ (‰)	(–25.57)–(–12.57) av = –21.81	(–26.63)–(–14.76) av = –22.03	(–26.47)–(–23.63) av = –24.88
	Gypsum ($n = 8$)	Selenite $\delta\text{S}_{\text{CDT}} = 17.7\text{‰}$ $\sigma = 0.5\text{‰}$ $\delta\text{S}_{\text{CDT}} = -5.8\text{‰}$, –39.4‰	Calcite pseudomorphs after gypsum rosettes Low	Calcite pseudomorphs after gypsum rosettes Low
Associated minerals	Pyrite	Not found	Common. Associated with dolomite and feldspar	Common. Associated with dolomite and feldspar
	Barite	Not found	Restricted to calcite pseudomorphs	Restricted to calcite pseudomorphs
	Celestite	Common. Associated with dolomite		

Perfect crystallinity=1.0.

Data for dolomite and pyrite taken from Sanz-Montero et al. (2006b) and Sanz-Montero et al. (2009), respectively.

and are often bonded together by carbonaceous membranes forming honeycomb-like frameworks or filament-like structures (Fig. 7). Poorly crystallised dolomite crystals show granular to spheroidal external morphologies. Spheroid-like crystals commonly exhibit distinctive C-rich or empty cores (Fig. 8). Previous studies by Sanz-Montero et al. (2006a), Ayllón-Quevedo et al. (2007), and Sanz-Montero et al. (2008) suggested that these types of crystals arose from the epicellular precipitation of dolomite on bacteria.

TOC determinations detect the presence of up to 0.3 wt.% of organic carbon in the samples (Table 1). The isotopic composition of the insoluble organic residue yielded $\delta^{13}\text{C}_{\text{PDB}}$ average values between -24.88% and $-21.81\pm 0.15\%$.

Data from Sanz-Montero et al. (2006b) indicate that the carbonate contains invariably poorly-ordered (av. 0.4) calcian dolomites ranging in composition from 49 to 55 mol% CaCO_3 (av. 51%). Average $\delta^{13}\text{C}$ values of dolomites in the three successions range from -6.6% to -4.6% (PDB), and average $\delta^{18}\text{O}_{\text{PDB}}$ values of the dolomites oscillate from -3.3% to -0.3% (Table 1). In some dolostone beds, dolomite crystals occur intergrown with framboidal pyrite clusters. The pyrite ($\delta^{34}\text{S}_{\text{CDT}} = -5.8\%$ and -39.4%) is significantly depleted in ^{34}S relative to the associated gypsum, with an average $\delta^{34}\text{S}_{\text{CDT}}$ value of 17.7% , standard deviation $= 0.5\%$ (Sanz-Montero et al., 2009).

4.2. Celestite and barite occurrences

Variable quantities, generally lower than 5%, of barite and/or celestite are associated with dolomite. The composition and distribution of these sulphates vary in the different sedimentary sequences

(Table 1). In the lower succession from the Madrid Basin (S1), only celestite is found associated with dolomite. Barite is the dominant sulphate in the two other sedimentary sequences (S2 and S3), whereas scarce celestite crystals are exclusively associated with the calcite cements that fill gypsum moulds.

4.2.1. Celestite

Three types of celestite occurrences have been found. Type 1 celestite crystals occur as single or, more commonly, intergrown clusters, concentrated in pockets and cracks, and hosted in dolomite interbedded with selenite gypsum (Fig. 9). Pockets have nodular and vug morphologies likely created by the dissolution of an anhydrite precursor. This interpretation is supported by the presence of gypsum nodules after anhydrite in the same range of sizes and morphologies throughout the facies association (Fig. 3). Celestite aggregates of subhedral prismatic crystals up to $50\text{ }\mu\text{m}$ long and $10\text{ }\mu\text{m}$ wide (Fig. 10) have transitional boundaries with openly-packed dolomite crystals. Celestite is nucleated on luminescent carbonaceous films (Fig. 10B) as poorly defined crystals that increase significantly their crystallinity outwards from the nucleation surfaces (Fig. 10C and D). The organic films embedding the precipitates commonly form bridges spanning the spaces between adjacent dolomite or celestite crystals (Fig. 10C and D). EMP results indicate that the celestite crystals contain BaO (b4.5 wt.%). Variable amounts of Si, Al, S, Sr, and Ca are detected in the carbonaceous films.

The second type of celestite is found as single crystals throughout the dolomite patches replacing selenite gypsum (Fig. 8B). Celestite is relatively pure (containing 0.9–2.5 wt.% BaO, 0.2–0.4 wt.% CaO, and MgO b0.1 wt.%). This type occurs as subhedral to euhedral crystals

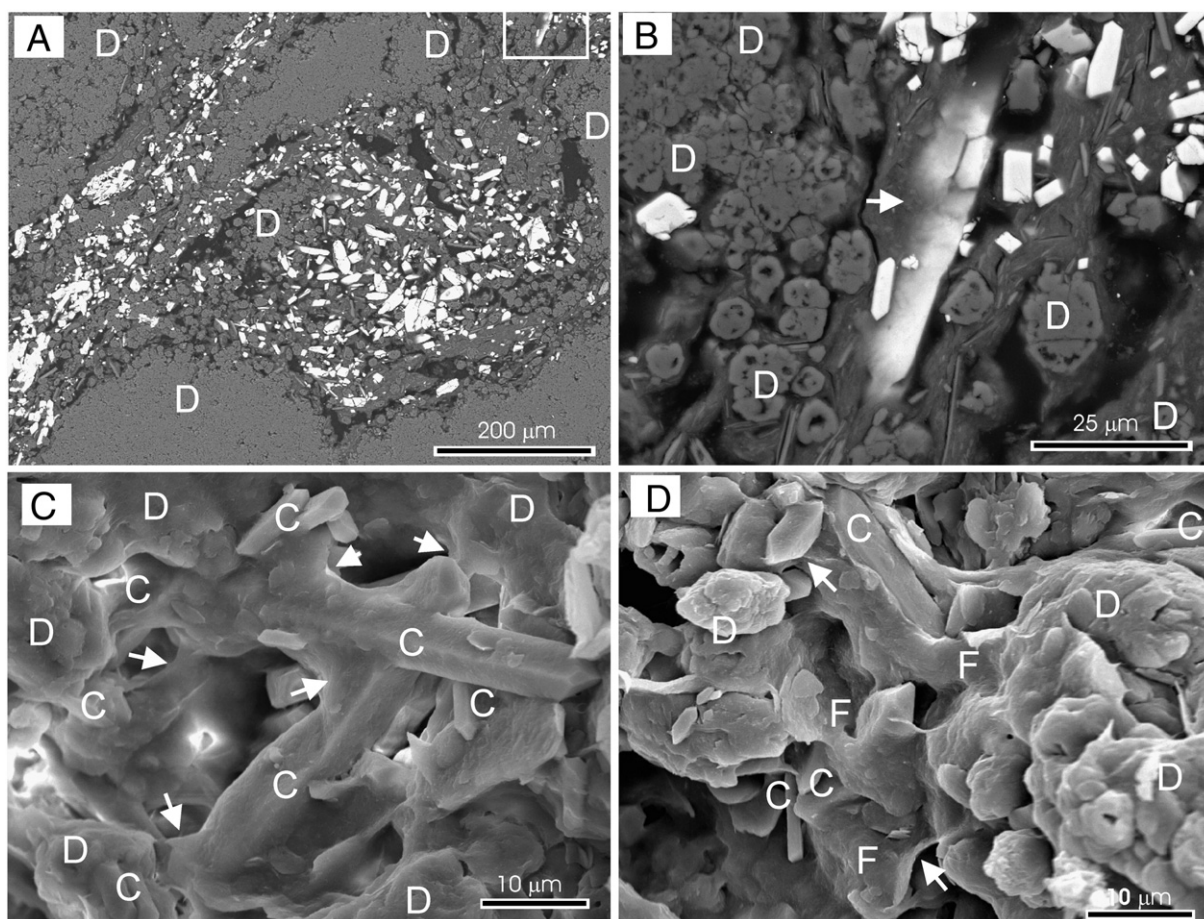


Fig. 10. SEM images of celestite clusters concentrated in pockets. A and B—SEM-BSE images of thin sections. C and D—SEM images of freshly-broken samples. A) Subhedral prismatic celestite crystals in pockets (white crystals) have very variable sizes and are mixed with dolomite (D). B) Magnified image of square area in A showing a gradual boundary between celestite (white crystals) and C-rich films (arrowed). C) The crystallinity of celestite increases from the organic nucleation surfaces towards the pores. Distances between adjacent dolomite (D) and celestite crystals (C) are spanned by bridges of carbonaceous films (arrowed). D) Celestite (C) and coeval dolomite (D) are embedded in the organic films (F).

exhibiting prismatic, some doubly terminated, forms up to 125 μm long and 50 μm wide (Fig. 11). Celestite crystals are commonly intergrown with dolomierite and embedded in carbonaceous masses (Fig. 11A) that Sanz-Montero et al. (2006a) attributed to fossil extracellular polymeric substances (EPS). These authors also found that the associated organic matter bound appreciable quantities of Mg and Ca, and, locally, even Sr.

Type 3 embraces the celestite included in gypsum moulds backfilled by calcite cements in S2 and S3 (Fig. 12A and B). These occur as single prismatic and tabular crystals up to 25 μm , mostly associated with minor dolomite, and corroded by calcite cements (Fig. 12B). Patchy barite and spherulite-like calcite crystals, commonly poikilitic, are concentrated in the proximity of the gypsum pseudomorphs (Figs. 8A and 12C), and disappear progressively with distance. Spherulite-like calcite crystals have grown outwards from the outer edges of the precursor gypsum, whereas drusy cements of calcite precipitated inwards from those surfaces (Fig. 12A). The relationships and gradual transitions recognised between the two types of calcite crystals thus suggest coevality. EMP analyses of the cements detect the presence of minor SrO (b1 wt.%) and a lack of Ba in calcite crystals infilling the moulds. The spherulite-like calcite precipitated in the vicinity of the moulds lacks Sr and contains some BaO (b1 wt.%).

4.2.2. Barite

Two main types of barite, single and aggregate crystals, are found throughout the dolostone microbialites associated with the intrase-

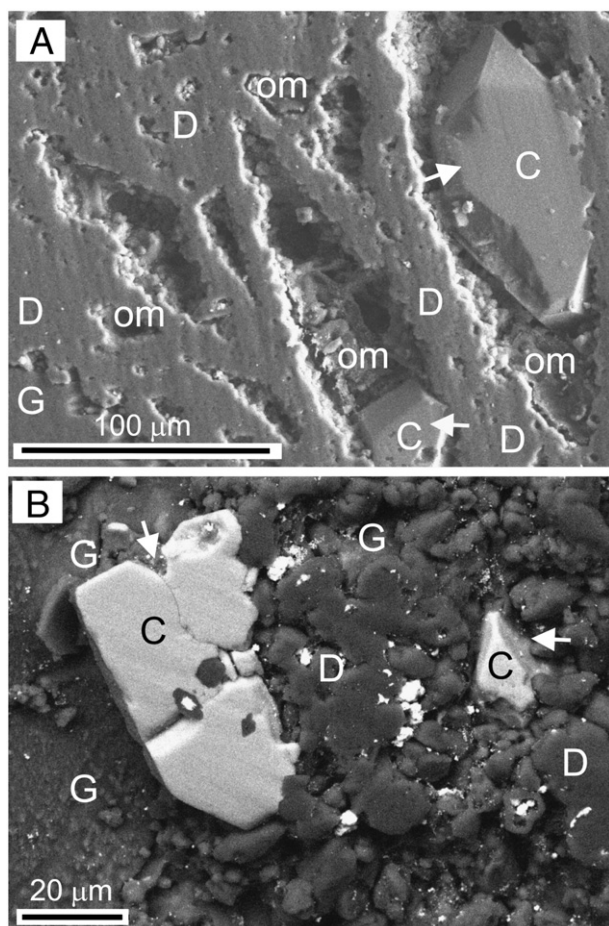


Fig. 11. SEM-SE (A) and SEM-BSE (B) thin-section photomicrographs of celestite (C, some arrowed) and dolomite (D) replacing selenite gypsum (G). A) Image of orthorhombic, double-terminated, celestite crystals closely associated with amorphous organic matter (om) in lenticular gypsum moulds. B) Dolomite and celestite (white minerals) occur tightly interlocked. Notice dolomite crystals encased by the big celestite crystal that is replacing the gypsum on the left.

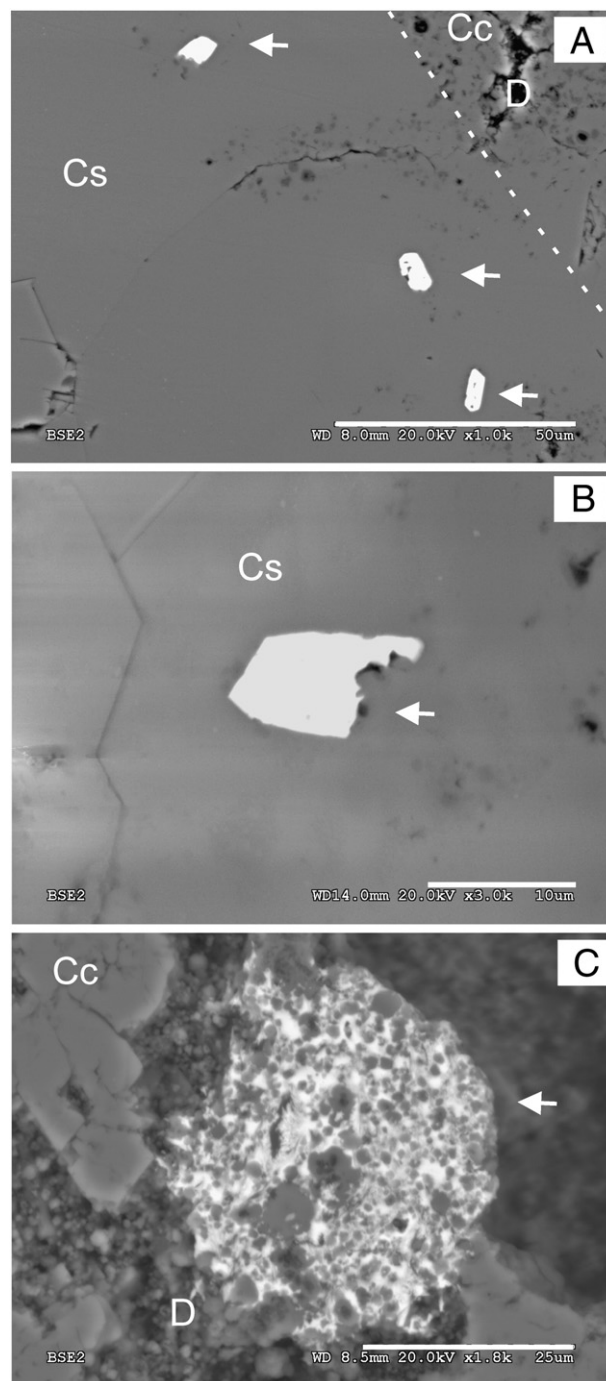


Fig. 12. SEM-BSE photographs of barite and celestite related to calcite after intra-sedimentary rosette-like gypsum. A) Celestite crystals (arrowed) are interspersed in the calcite cement (Cs) precipitated within a gypsum mould; the dashed line indicates the precursor gypsum edge. Spherulite-like calcite precipitates (Cc) are also found in the dolomite matrix (D) embedding the gypsum pseudomorphs. Scale bar 50 μm . B) Detail of celestite (arrowed) encased by calcite cements (Cs). Scale bar 10 μm . C) Magnification of the dolomite matrix (D) and associated calcite crystals (Cc) in the vicinity of the pseudomorphs. A subhedral barite crystal (arrowed) encloses numerous spheroidal dolomite crystals. Scale bar 25 μm .

dimentary gypsum pseudomorphs (Fig. 12C). Barite crystals are nucleated on the carbonate host that consists of submicron to micrometre-sized dolomite precipitates glued together by organic substances (Figs. 8A, 12C and 13). Barite is relatively pure (containing 2.5–3.6 wt.% SrO, 0.7–5.0 wt.% CaO and 0.0–1.1 wt.% MgO).

Single anhedral to subhedral tabular barite crystals, up to 50 μm long and 15 μm wide, precipitated as patchy poikilitic cements, which include

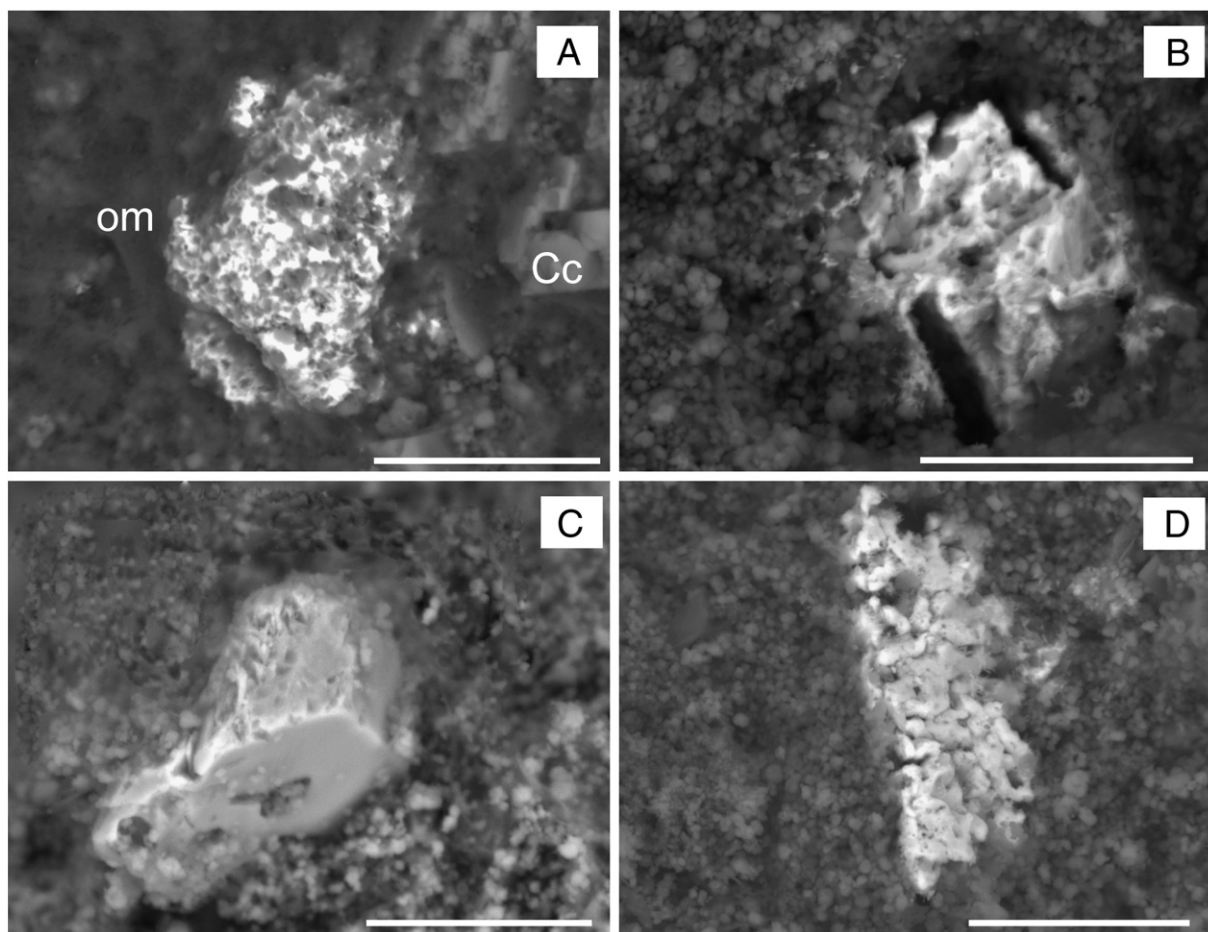


Fig. 13. SEM-BSE images of uncoated polished samples showing barite nucleated on the dolomite matrix. A) A poikilitic barite crystal coexisting with calcite crystals (Cc) is embedded in organic matter films (om). B) A poikilitic barite crystal includes poorly crystallised dolomicrite and filament-like moulds. C) Tabular barite nucleated on the dolomite matrix exhibits well crystallised habits outwards from the nucleation sites. D) Barite precipitate composed of rounded to ellipsoidal crystallites showing irregular outlines. Scale bar 20 μm .

up to 60% of dolomicrite, filament-like moulds and, even, carbonaceous masses from the matrix (Fig. 13A and B). Poorly defined transitions are observed between the barite and the nucleation substrate, although outwards the crystals exhibit well-crystallised habits (Figs. 12C and 13C). Barite is mostly associated with the calcite precipitated in the vicinity of the gypsum pseudomorphs (Figs. 12C and 13A).

Less abundant are the up to 30 μm long and 10 μm wide irregular barite crystals composed of 1–3 μm sized crystallite aggregates (Fig. 13D). Dolomicritic matrix forms both the outlines and the cores of the rounded to ellipsoidal crystallites of barite.

Barite is subordinately found as secondary products in pits and galleries developed inside weathered K-feldspar within the dolomite matrix (Fig. 14A). Barite consists of up to 50 μm long and 30 μm wide subhedral crystals with low SrO contents (0.11–0.25 wt.%). The sulphate precipitates can be embedded in Ba and S-bearing carbonaceous substances (Fig. 14B). The BaO content in the host feldspars ranges from 0.09 to 0.42 wt.%.

5. Interpretation and discussion

On the basis of petrographical, mineralogical, isotope, and facies assemblage analyses, Sanz-Montero et al. (2006a) and Sanz-Montero et al. (2008) interpreted the dolostone beds as microbialites resulting from the mineralization of microbial mats in saline lake margins. The term microbialite is used in the sense of Burne and Moore (1987), describing an organosedimentary deposit formed from the interaction between benthic microbial communities and detrital or chemical sedi-

ments. Bedded gypsum accumulated in the lake from a brine of moderate salinity between 20 and 90 g/L NaCl (Ayllón-Quevedo et al., 2007). Intrasedimentary lenticular and rosette-like gypsum crystallised from interstitial brine within dolomite sediments (Sanz-Montero et al., 2008). In contrast, depleted ^{18}O isotopic values in the dolomite (ranging from an average minimum of -3.3‰ to -0.3‰) exclude evaporation as a main formative process and indicate that the carbonate precipitated from relatively dilute water (Sanz-Montero et al., 2006a). In these sedimentary contexts, the alluvial-fans episodically supplied the mudflat-marginal lake fringes with detrital grains that were trapped and bound to the mats. Sanz-Montero et al. (2008) suggested that the nucleation of dolomite took place in the microbial mats thriving in Miocene lacustrine systems as the organic matter decayed through bacterial sulphate reduction processes. The organic substrate favoured dolomite precipitation providing suitable nucleation sites and appropriate geochemical conditions (e.g., concentration of Mg) to allow minerals to nucleate. The isotope signature (average $\delta^{13}\text{C}_{\text{PDB}}$ values ranging from -24.88‰ to -21.88‰) of the organic carbon (kerogen) from the studied microbialites is likewise consistent with its microbial origin (Konhauser, 2007). Consequently, Miocene celestite and barite co-precipitated with microbially mediated dolomite in lacustrine environments under relatively dilute conditions, which preclude an evaporative origin for the sulphates.

Although a complete solid solution series exists between barite and celestite, most barite contains less than 7 mol% SrSO_4 and most celestite contains less than 4 mol% BaSO_4 (Hanor, 2000). The extremely low solubility of BaSO_4 compared with SrSO_4 , implies that barite

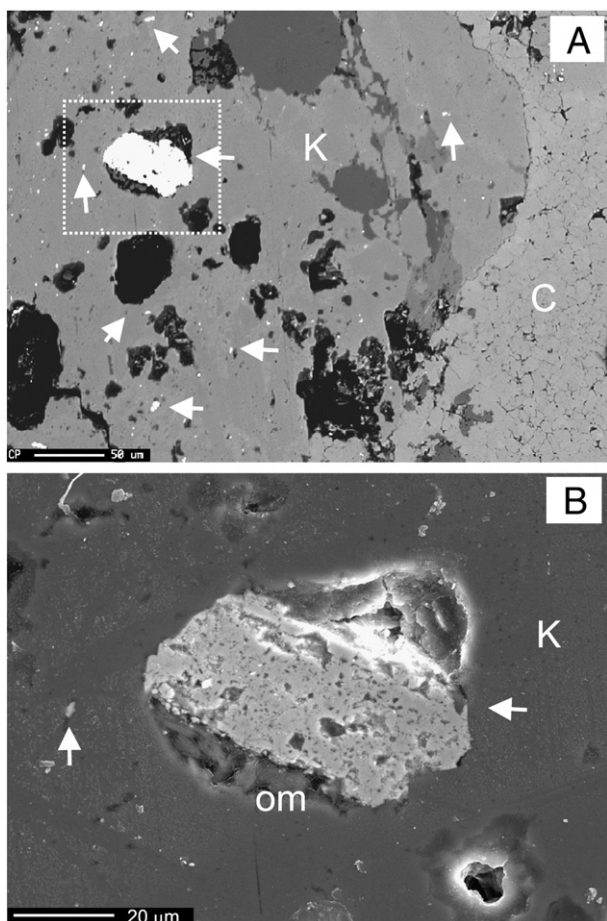


Fig. 14. SEM-BSE images of barite precipitates in deeply weathered K-feldspars (K) scattered in the carbonate matrix (C). A) Barite crystals of varied sizes (some arrowed) abound in the weathered feldspar. B) Detailed image of the square area in A showing a barite crystal that coexists with organic substances (om) in a pit.

precipitates preferentially even at very low concentrations of Ba (Felmy et al., 1993), and the aqueous phase must be very poor in Ba in precipitating strontium-rich solid solutions (Prieto et al., 1997).

The extent of gypsum replacement by dolomite in the study case S1 in which gypsum is more abundant, and the former presence of gypsum, only indicated by calcite pseudomorphs in the two other situations (S2 and S3), certainly point out that the SO_4^{2-} required for barite and celestite formation was remobilized from the sedimentary gypsum. Bacterial sulphate reduction is considered by many authors (e.g., Pierre and Rouchy, 1988; Anadón et al., 1992; Taberner et al., 2002) as the main process responsible for the replacement of sulphates by carbonates and related reactions at low temperatures. Although calcite is the common carbonate resulting from sulphate reduction processes (Machel, 2001), different studies on recent sediments from coastal areas have also shown that bacterial sulphate reduction is further involved in the formation of dolomite (Vasconcelos and McKenzie, 1997; Wright, 1999; Wright and Wacey, 2005). Additionally, Sanz-Montero et al. (2006a) attributed the replacement of selenite gypsum in S1 to the microbial corrosion of gypsum and concomitant dolomite precipitation. Depleted $\delta^{34}\text{S}$ values in the pyrite relative to the associated gypsum further indicate that sulphate microbial reduction to sulphide played a role in gypsum dissolution. Low $\delta^{13}\text{C}$ values (av. -8.48‰ PDB) in calcite pseudomorphs after gypsum reported by Sanz-Montero et al. (2005) in the Duero Basin deposits indicate that bacterial sulphate reduction is also a plausible explanation for the removal of intrasedimentary gypsum in solution and sub-sequent calcite precipitation. These processes may have taken place early in the sedimentary environment as the presence of the

poikilotropic spherulite-like calcite crystals suggests. The poikilotropic crystals fill the interparticle porosity developed within the open dolomite framework (Fig. 8A), which argues for slow crystal growth in sustained phreatic conditions within the unconsolidated sediment. Similar pseudospherulite-like calcite crystals in Tertiary successions have been further interpreted as early-diagenetic paleogroundwater products by Rossi and Cañaveras (1999).

The close association of barite with Ba-bearing feldspars and the abundance of deeply weathered feldspars in the dolomite micro-bialites suggest that feldspar weathering, probably caused by microbial activity (Sanz-Montero and Rodríguez-Aranda, 2009), was a major source of Ba for barite. Along similar lines, and in view of the links of celestite with gypsum in the Lower Unit of the Madrid Basin (S1), Rodríguez-Aranda et al. (2005) concluded that the Sr for celestite was released from the associated gypsum, whose Sr content ranges 928–1832 ppm (Rodríguez-Aranda, 1995). The lack of any remaining gypsum in the two other sequences makes it impossible to determine its precise composition, although primary gypsum in the Madrid Basin is characterised by high Sr contents (Fort and Bustillo, 1986). The presence of Sr in calcite precipitated in the gypsum moulds and the lack of this element in coeval calcite precipitated externally, also support gypsum-sourced strontium in these sequences.

Taking into account the moderately high levels of sulphate and high Sr/Ba ratios required in the celestite-forming solutions (Hanor, 2004); the calcium sulphate Sr source may explain why celestite is restricted to microenvironments created within gypsum or anhydrite precursors, whereas barite, if present, coexists in the vicinity. Barite and celestite show a patchy distribution in constrained microenvironments with abundant organic substances on which the crystals nucleated. Assuming the formative environment in microbial mats, the organic substances are thought to represent fossil extracellular polymeric substances (EPS). The association of these substances with dolomite crystals precipitated epicellularly on bacteria (Ayllón-Quevedo et al., 2007; Sanz-Montero et al., 2008) and the isotope signature of the organic carbon further support this biological origin. Miocene barite and celestite thus are interpreted as precipitates on microbial EPS. Both barite and celestite nucleation on bacterial EPS have been reported in different continental sulphur-rich environments, including saline

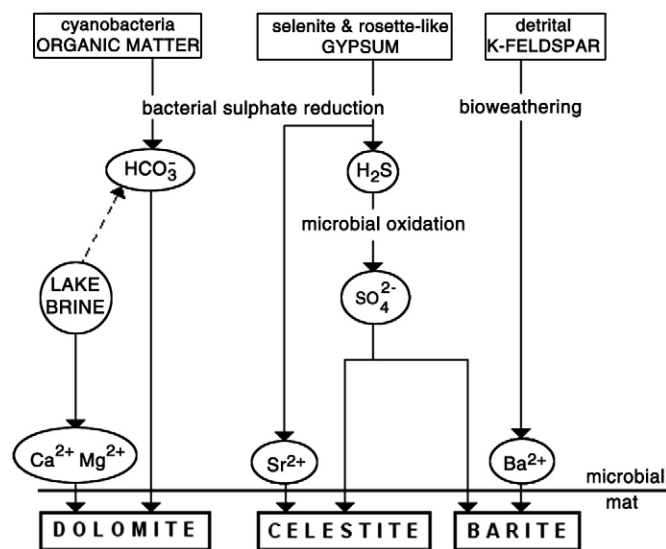


Fig. 15. Schematic model showing the interrelated pathways for the formation of sulphates and dolomite coupled with the weathering of feldspars deposited in microbial mats. Soluble barium can be released from the feldspars. Sulphide and/or sulphur and soluble strontium is provided by bacterial sulphate reduction of calcium sulphates and then reprecipitated as barite and celestite by bacterial oxidation of sulphide to sulphate. The microbial mat provides suitable nucleation sites and appropriate geochemical conditions (e.g., concentration of cations) to allow minerals to nucleate. The solid phases are in squares and the dissolved ones in circles.

lakes (Schultze-Lam and Beveridge, 1994; Douglas and Yang, 2002; Sánchez-Moral et al., 2004; Bonny and Jones, 2007). Nucleation on EPS embedding bacterial cells explains the inclusion of microbial structures (e.g., filament-like moulds, spheroidal dolomite crystals, and organic substances) in the poikilotopic crystals of barite. Although uncommon, poikilotopic cements of barite enclosing microbial structures have been reported in Albian microbialites by Bréhéret and Brumsack (2000) and in sulphur spring microbialites by Bonny and Jones (2007, 2008). The latter also pointed out that barite precipitates around microbial structures provide conclusive evidence for the role of microbes in its formation.

Mineral formation on bacterial surfaces is well established (i.e., Schultze-Lam et al., 1993). Microbial cells and EPS host electrostatically negatively-charged groups that can interact with metal ions, such as Sr^{2+} or Ba^{2+} , present in the aqueous surroundings. Subsequently, sulphates can form at nucleation sites between Sr^{2+} or Ba^{2+} and excess SO_4^{2-} from the fluid phases. Once the barrier to crystal nucleation is passed, the precipitates can grow abiotically, and form well-crystallised habits (González-Muñoz et al., 2003) as those found in the Miocene barite and celestite. On the basis of experimental studies, Bonny and Jones (2008) concluded that biogenic textures in barites precipitated on outer cell surfaces of bacteria and associated EPS develop under anoxic–dysoxic conditions. The authors also observed that multiple barite crystal habits can co-precipitate in close proximity.

Cluster aggregation and crystal elongation found in celestite precipitated in those pockets attributed to dissolution of intrasedimentary precursors, likely anhydrite, appear to be features of crystallisation at high supersaturation (Sunagawa, 1995). By contrast, the precipitation of single crystals of celestite in gypsum indicates lower levels of saturation, which is coherent with its formation in pits and boreholes produced by bacterial activity in the selenite crystals (Sanz-Montero et al., 2006a).

The transformation of reduced sulphur (previously produced by sulphate reducers) to oxidized forms (sulphate for barite or celestite) may have occurred abiotically or may have been mediated by sulphide oxidizing microbes as reported to take place in modern environments (Douglas and Yang, 2002; Senko et al., 2004). Rather than caused by pure abiotic processes, patchy distribution observed in the Miocene samples suggests that the precipitation of the sulphates took place in microenvironments and chemical gradients typically created by a specific bacterial type in microbial mats (Douglas, 2005). The coupling between sulphide oxidation by microbes and bacterial sulphate reduction further may have produced the chemical conditions necessary for dolomite precipitation, as documented at Brejo do Espinho, Brazil (Moreira et al., 2004).

In S2 and S3, barite often encases dolomite crystals postdating its precipitation. Further barite and dolomite growth was precluded by the coprecipitation of pervasive calcite cements. The bacterial reduction of intrasedimentary gypsum provided S and Ca to pore waters. Coeval release of metabolic C during bacterial sulphate reduction of organic matter may have led to calcite supersaturation and concomitant precipitation of spherulite-like calcite in the gypsum proximity.

Barite and celestite are thus thought to nucleate on Ba- or Sr-enriched EPS under conditions of sulphate supersaturation, the sulphate anion being likely derived by the microbial oxidation of reduced sulphur to sulphate (Fig. 15). The processes of sulphide oxidation and sulphate reduction also favoured the concomitant formation of dolomite (Moreira et al., 2004). It is also suggested that biologically weathered feldspars acted as a major source of Ba for barite, whereas Sr was released from gypsum and anhydrite deposits through the activity of sulphate reducing bacteria.

6. Conclusions

This research extends the record of biomediated barite and celestite occurrences to ancient rocks and gives insight into the interrelated

pathways that lead to the formation of Ba–Sr sulphates and dolomite. Three Miocene sedimentary successions bearing dolomite microbialites from the Duero and Madrid Basins contain celestite and/or barite. The composition and distribution of these sulphates in dolomites vary. Celestite is the only Ba–Sr sulphate present in one of the successions in which dolomite is interbedded with laterally continuous gypsum (S1). In the two other sedimentary successions (S2 and S3), single celestite crystals are restricted to calcite pseudomorphs after gypsum hosted in dolomite beds, while barite precipitates are found in the vicinity of the pseudomorphs.

The Ba–Sr sulphates formed in close proximity to the source of the S that was likely remobilized from the associated calcium sulphates through microbial sulphate reduction. The calcium sulphate-sourced strontium also explains the distribution of celestite and barite. In contrast, barium was released from deeply weathered Ba-bearing feldspar. The transformation of reduced sulphur (produced by sulphate reducers) to oxidized forms (sulphate for barite or celestite) may have been mediated by sulphide oxidizing microbes as supported by the patchy and localised distribution. The processes of sulphide oxidation and sulphate reduction also favoured the concomitant formation of dolomite. Patchy-distributed celestite and barite crystals were nucleated on organic substances, likely EPS, and commonly encase microbial structures which further provide evidence for the role of microbes in its formation.

Subsequent diagenetic evolution of the successions has apparently produced no major changes in the nature of these minerals, which confirms that the microbial signatures can be preserved in the geological record.

Acknowledgements

This work was funded by Projects PR34/07-15900 (Santander-Complutense) and CCG07-UCM/AMB-2299 (Comunidad de Madrid-Complutense). We are indebted to the guest scientific editor (Dr. C. Arenas) and the two reviewers (Drs. I. Armenteros and S. Douglas) for their valuable comments on the previous draft. Thanks to guest editor (Dr. E. Gierlowski-Kordesch) for detailed correction of the English text.

References

- Anadón, P., Rosell, L., Talbot, M.R., 1992. Carbonate replacement of lacustrine gypsum deposits in two Neogene continental basins, eastern Spain. *Sedimentary Geology* 78, 201–216.
- Arenas, C., Gutiérrez, F., Osacar, C., Sancho, C., 2000. Sedimentology and geochemistry of fluvio-lacustrine tufa deposits controlled by evaporite solution subsidence in the central Ebro Depression, NE Spain. *Sedimentology* 47, 883–909.
- Armenteros, I., Corrochano, A., Alonso-Gavilán, G., Carbalreira, J., Rodríguez, J.M., 2002. Duero Basin (northern Spain). In: Gibbons, W., Moreno, M.T. (Eds.), *The Geology of Spain*. In: *The Geological Society, London*, pp. 309–315.
- Ayllón-Quevedo, F., Souza-Egipsy, V., Sanz-Montero, M.E., Rodríguez-Aranda, J.P., 2007. Fluid inclusion analysis of twinned selenite gypsum beds from the Miocene of the Madrid basin (Spain). Implication on dolomite bioformation. *Sedimentary Geology* 201, 212–230.
- Bonny, S.M., Jones, B., 2007. Diatom-mediated barite precipitation in microbial mats calcifying at Stinking Springs, a warm sulphur spring system in Northwestern Utah, USA. *Sedimentary Geology* 194, 223–244.
- Bonny, S.M., Jones, B., 2008. Experimental precipitation of barite (BaSO_4) among streamers of sulfur-oxidizing bacteria. *Journal of Sedimentary Research* 78, 357–365.
- Bréhéret, J.G., Brumsack, H.J., 2000. Barite concretions as evidence of pauses in sedimentation in the Marnes Bleues Formation of the Vocontian Basin (SE France). *Sedimentary Geology* 130, 205–228.
- Burne, R.V., Moore, L.S., 1987. Microbialites organosedimentary deposits of benthic microbial communities. *Palaos* 2, 241–254.
- Calvo, J.P., Alonso-Zarza, A.M., García del Cura, M.A., Ordóñez, S., Rodríguez-Aranda, J.P., Sanz-Montero, M.E., 1996. Sedimentary evolution of lake systems through Miocene, Madrid Basin. Paleoclimatic and Paleohydrological constraints. In: Friend, P., Dabrio, C. (Eds.), *Tertiary Basins of Spain*. In: *Cambridge University Press, Cambridge*, pp. 264–269.

Douglas, S., 2002. ESEM-EDS and XRD study of micromineralogical layering in a microbial mat from a hypersaline pond on Lee Stocking Island, Bahamas: formation of celestite in microbial exopolymers. Annual meeting of the Geological Society of America. Abstracts.

- Douglas, S., 2005. Mineralogical footprints of microbial life. *American Journal of Science* 305, 503–525.
- Douglas, S., Yang, H., 2002. Mineral biosignatures in evaporites: presence of rosickyite in an endoevaporitic microbial community from Death Valley, California. *Geology* 30, 1075–1078.
- Felmy, A.R., Rai, D., Moore, D.A., 1993. The solubility of (Ba, Sr)SO₄ precipitates: thermodynamic equilibrium and reaction path analysis. *Geochimica et Cosmochimica Acta* 57, 4345–4363.
- Fort, R., Bustillo, M., 1986. Estudio geoquímico de los yesos miocenos de la zona Este de la Cuenca de Madrid. *Estudios Geológicos* 42, 387–395.
- González-Múñoz, M.T., Fernández-Luque, B., Martínez-Ruiz, F., Chekroun, K.B., Arias, J.M., Rodríguez-Gallego, M., Martínez-Canamero, M., de Linares, C., Paytan, A., 2003. Precipitation of Barite by *Myxococcus xanthus*: possible implications for the biogeochemical cycle of barium. *Applied and Environmental Microbiology* 69, 5722–5725.
- Grassineau, N.V., 2006. High-precision EA-IRMS analysis of S and C isotopes in geological materials. *Applied Geochemistry* 21, 756–765.
- Hanor, L.S., 2000. Barite-celestine geochemistry and environments of formation. *Reviews in Mineralogy and Geochemistry* 40, 193–275.
- Hanor, L.S., 2004. A model for the origin of large carbonate- and evaporite-hosted celestine (SrSO₄) deposits. *Journal of Sedimentary Research* 74, 168–175.
- Kaiser, C.J., Kelly, W.C., Wagner, R.J., Shanks, W.C., 1987. Geologic and geochemical controls of mineralization in the southeast Missouri barite district. *Economic Geology* 82, 719–734.
- Konhauser, K., 2007. *Introduction to Geomicrobiology*. Blackwell Publishing, 425 pp.
- Machel, H.G., 2001. Bacterial and thermochemical sulphate reduction in diagenetic setting—old and new insights. *Sedimentary Geology* 140, 143–175.
- Moreira, N.L., Walter, L.M., Vasconcelos, C., McKenzie, J.A., McCall, P.J., 2004. Role of sulfide oxidation in dolomitization: sediment and pore-water geochemistry of a modern hypersaline lagoon system. *Geology* 32, 701–704.
- Pierre, C., Rouchy, J.M., 1988. Carbonate replacements after sulfate evaporites in the middle Miocene of Egypt. *Journal of Sedimentary Petrology* 58, 446–456.
- Plummer, L.N., 1971. Barite deposition in Central Kentucky. *Economic Geology* 66, 252–258.
- Prieto, M., Fernández-González, A., Putnis, A., Fernández-Díaz, L., 1997. Nucleation, growth, and zoning phenomena in crystallizing (Ba,Sr)CO₃, Ba(SO₄,CrO₄), (Ba,Sr)SO₄, and (Cd,Ca)CO₃ solid solutions from aqueous solutions. *Geochimica et Cosmochimica Acta* 61, 3383–3397.
- Rodríguez-Aranda, J.P., 1995. *Sedimentología de los sistemas de llanura lútica-lago salino del Mioceno en la zona oriental de la Cuenca de Madrid (Tarancón-Auñón)*. Ph.D. Thesis. Universidad Complutense, Madrid, Spain.
- Rodríguez-Aranda, J.P., Rouchy, J.M., Calvo, J.P., Ordóñez, S., García del Cura, M.A., 1995. Unusual twinning features in large primary gypsum crystals formed in salt lake conditions, Middle Miocene, Madrid Basin, Spain—palaeoenvironmental implications. *Sedimentary Geology* 95, 123–132.
- Rodríguez-Aranda, J.P., Calvo, J.P., Sanz-Montero, M.E., 2002. Lower Miocene gypsum palaeokarst in the Madrid Basin (central Spain): dissolution, diagenesis, morphological relics and karst end-products. *Sedimentology* 49, 1385–1400.
- Rodríguez-Aranda, J.P., Sanz-Montero, M.E., Ayllón-Quevedo, F., Souza-Egipsy, V., 2005. Formación de celestina dentro de un contexto microbiano en ambiente lacustre salino. Mioceno Inferior de la Cuenca de Madrid. *Macla* 3, 171–172.
- Rossi, C., Cañaveras, J.C., 1999. Pseudospherulitic fibrous calcite in paleo-groundwater, unconformity-related diagenetic carbonates (Paleocene of the Áger basin and Miocene of the Madrid basin, Spain). *Journal of Sedimentary Research* 69, 224–238.
- Sanz-Montero, M.E., Rodríguez-Aranda, J.P., 2009. Silicate bioweathering and biomineralization in lacustrine microbialites: ancient analogues from the Miocene Duero basin. *Geological Magazine* 146, 527–539. (Published online by Cambridge University Press 03 Feb 2009).
- Sánchez-Moral, S., Luque, L., Cañaveras, J.C., 2004. Bioinduced barium precipitation in St. Callixtus and Domitilla catacombs. *Annals of Microbiology* 54, 1–12.
- Sanz-Montero, M.E., Rodríguez-Aranda, J.P., García del Cura, M.A., 2005. Texturas diagenéticas de calcita desarrolladas sobre facies dolomíticas microbianas en el Mioceno de la Cuenca del Duero (zona de Cuéllar). *Macla* 3, 193–195.
- Sanz-Montero, M.E., Rodríguez-Aranda, J.P., Calvo, J.P., 2006a. Mediation of endoevaporitic microbial communities in early replacement of gypsum by dolomite: a case study from Miocene lake deposits of the Madrid Basin, Spain. *Journal of Sedimentary Research* 76, 1257–1266.
- Sanz-Montero, M.E., García del Cura, M.A., Rodríguez-Aranda, J.P., 2006b. Facies dolomíticas de sistemas lacustres miocenos en las cuencas del Duero y de Madrid. Rasgos indicativos de su origen microbiano. *GeoTemas* 9, 205–208.
- Sanz-Montero, M.E., Rodríguez-Aranda, J.P., García del Cura, M.A., 2008. Dolomite-silica stromatolites in Miocene lacustrine deposits from the Duero Basin, Spain: the role of organotemplates in the precipitation of dolomite. *Sedimentology* 55, 729–750.
- Sanz-Montero, M.E., Rodríguez-Aranda, J.P., Pérez-Soba, C., 2009. Microbial weathering of Fe-rich phyllosilicates and formation of pyrite in the dolomite precipitating environment of a Miocene lacustrine system. *European Journal of Mineralogy* 21, 163–175.
- Schultze-Lam, S., Beveridge, T.J., 1994. Nucleation of celestite and strontianite on a cyanobacterial S-layer. *Applied and Environmental Microbiology* 60, 447–453.
- Schultze-Lam, S., Douglas, T., Thompson, J.B., Beveridge, T.J., 1993. Metal ion immobilization by bacterial surfaces in freshwater environmental. *Water Pollution Research Journal of Canada* 28, 51–81.
- Senko, J.M., Campbell, B.S., Henriksen, J.R., Elshahed, M.S., Dewers, T.A., Krumholz, L.R., 2004. Barite deposition resulting from phototrophic sulphide-oxidizing bacterial activity. *Geochimica et Cosmochimica Acta* 68, 773–780.
- Sunagawa, I. (Ed.), 1995. *Morphology of crystals*. In: Kluwer, Tokyo. 419 pp.
- Taberner, C., Marshall, J.D., Hendry, J.P., Pierre, C., Thirlwall, M.F., 2002. Celestite formation, bacterial sulphate reduction and carbonate cementation of Eocene reefs and basinal sediments (Igalada, NE Spain). *Sedimentology* 49, 171–190.
- Vasconcelos, C., McKenzie, J.A., 1997. Microbial mediation of modern dolomite precipitation and diagenesis under anoxic conditions (Lagoa Vermelha, Rio de Janeiro, Brazil). *Journal of Sedimentary Research* 67, 378–390.
- West, I., 1973. Vanished evaporites; significance of strontium minerals. *Journal of Sedimentary Research* 43, 278–279.
- Williams-Jones, A.E., Schrijver, K., Doig, R., Sangster, D.F., 1992. A model for epigenetic Ba–Pb–Zn mineralization in the Appalachian Thrust Belt, Quebec: evidence from fluid inclusions and isotopes. *Economic Geology* 87, 154–174.
- Wright, D.T., 1999. The role of sulphate-reducing bacteria and cyanobacteria in dolomite formation in distal ephemeral lakes of Coorong region, South Australia. *Sedimentary Geology* 126, 147–157.
- Wright, D.T., Wacey, D., 2005. Precipitation of dolomite using sulphate-reducing bacteria from the Coorong Region, South Australia: significance and applications. *Sedimentology* 52, 987–1008.